J|A|C|S ARTICLES

Published on Web 07/06/2009

Colorimetric Split G-Quadruplex Probes for Nucleic Acid Sensing: Improving Reconstituted DNAzyme's Catalytic Efficiency via Probe Remodeling

Shizuka Nakayama and Herman O. Sintim*

Department of Chemistry and Biochemistry, University of Maryland, College Park, Maryland 20742

Received April 14, 2009; E-mail: hsintim@umd.edu

Abstract: Split G-rich DNA probes can assemble into active peroxidase-mimicking DNAzymes in the presence of bioanalytes such as DNA, thereby providing a simple and cheap means to detect analytes in biological samples. A comprehensive study designed to reveal the salient probe architectural features and reaction conditions that facilitate facile reconstitution into enzymatically proficient enzymes unveiled these important findings: (a) The loops that connect the G3-tracts in a G-quadruplex structure can be replaced with a stem-loop or loop-stem-loop motif without destabilizing the resulting quadruplex structure; endowing the split G-rich probes with regions of limited complementarity leads to more proficient reconstituted enzymes. (b) The addition of hemin to antiparallel G-quadruplex DNAzymes lead to a blue shift in the CD spectra of the G-quadruplex DNAzymes. (c) The architectures of the DNA motifs that lie adjacent to the G-quadruplex structure influence both the stability and the enzymatic proficiency of the reconstituted enzymes. (d) The nature of the monovalent cation that is present in excess is a key determinant of the turnovernumber of the G-quadruplex DNAzyme; decomposition of G-quadruplex DNAzymes is slower in buffers that contain ammonium ions than those that contain sodium or potassium ions. These findings are important for the design of bioassays that use peroxidase-mimicking G-quadruplexes as detection labels.

Introduction

Biomedical devices or assays that can be used by physicians to detect disease markers at point-of-care or for large-scale screening programs will vastly improve our ability to predict or diagnose diseases at earlier stages, leading to enhancement of the quality of human life and also an increase in life expectancy. The majority of the assays[1] that are used to detect nucleic acids in patients' samples incorporate either the polymerase chain reaction (PCR)[2] or the ligase chain reaction (LCR).[3] Both PCR and LCR are however sensitive to sample quality and the presence of inhibitory substances in complex biological samples may interfere with PCR/LCR amplification.[4] PCR and LCR are also not ideal for the direct amplification of short nucleic acids such as microRNAs, which are emerging as important cancer biomarkers.[5] Additionally, both PCR and LCR require sophisticated instrumentation and skilled technicians thereby making them nonideal for point-of-care or economically disadvantaged areas or for field testing. Consequently, several groups have embarked on the development of cheap and shelf-stable nonprotein-based biomolecule detection platforms as alternatives to PCR and LCR-based assays.[6]

Recently the detection of DNA by probes that can reconstitute into active peroxidase-mimicking G-quadruplex DNAzymes (Figure 1),[7] has gained increasing popularity because these approaches afford a simple detection of nucleic acids via colorimetric means without the need for expensive proteins such

(1) (a) Holland, P. M.; Abramson, R. D.; Watson, R.; Gelfand, D. H. *Proc. Natl. Acad. Sci. U.S.A.* **1991**, *88*, 7276–7280. (b) Whitcombe, D.; Theaker, J.; Guy, S. P.; Brown, T.; Little, S. *Nat. Biotechnol.* **1999**, *17*, 804–807. (c) Chen, X.; Kwok, P. *Nucleic Acids Res.* **1997**, *25*, 347–353. (d) Lyamichev, V.; Mast, A. L.; Hall, J. G.; Prudent, J. R.; Kaiser, M. W.; Takova, T.; Kwiatkowski, R. W.; Sander, T. J.; de Arruda, M.; Arco, D. A.; Neri, B. P.; Brow, M. A. D. *Nat. Biotechnol.* **1999**, *17*, 292–296.

(2) Saiki, R. K.; Gelfand, D. H.; Stoffel, S.; Scharf, S. J.; Higuchi, R.; Horn, G. T.; Mullis, K. B.; Erlich, H. A. *Science* **1988**, *239*, 487–491.

(3) Barany, F. *Proc. Natl. Acad. Sci. U.S.A* **1991**, *88*, 189–193.

(4) (a) Lantz, P. G.; Matsson, M.; Wadström, T.; Rådström, P. J. *Microbiol. Methods* **1997**, *28*, 159–167. (b) Monteiro, L.; Bonnemaison, D.; Vekris, A.; Petry, K. G.; Bonnet, J.; Vidal, R.; Cabrita, J.; Mégraud, F. *J. Clin. Microbiol.* **1997**, *35*, 995–998. (c) Akane, A.; Matsubara, K.; Nakamura, H.; Takahashi, S.; Kimura, K. *J. Forensic Sci.* **1994**, *39*, 362–372. (d) Belec, L.; Authier, J.; Eliezer-Vanerot, M.; Piedouillet, C.; Mohamed, A.; Gherardi, R. *Muscle Nerve* **1998**, *21*, 1064–1067. (e) Al-Soud, W. A.; Rådström, P. *J. Clin. Microbiol.* **2001**, *39*, 485–493. (f) Al-Soud, W. A.; Jönsson, L. J.; Rådström, P. *J. Clin. Microbiol.* **2000**, *38*, 345–350.

(5) (a) Rifai, N.; Gillette, M. A.; Carr, S. A. *Nat. Biotechnol.* **2006**, *24*, 971–983. (b) Mitchell, P. S.; Parkin, R. K.; Kroh, E. M.; Fritz, B. R.; Wyman, S. K.; Pogosova-Agadjanyan, F. L.; Peterson, A.; Noteboom, J.; O'Briant, K. C.; Allen, A.; Lin, D. W.; Urban, N.; Drescher, C. W.; Knundsen, B. S.; Stirewalt, D. L.; Gentleman, R.; Vessella, R. L.; Nelson, P. S.; Martin, D. B.; Tewari, M. *Proc. Natl. Acad. Sci. U.S.A.* **2008**, *105*, 10513–10518. (c) Habbe, N.; Koorstra, J. B.; Mendell, J. T.; Offerhaus, G. J.; Ryu, J. K.; Feldmann, G.; Mullendore, M. E.; Goggins, M. G.; Hond, S. M.; Maitra, A. *Cancer Biol. Ther.* **2009**, *8*, 340–346.

(6) (a) Abe, H.; Kool, E. T. *J. Am. Chem. Soc.* **2004**, *126*, 13980–13986. (b) Grossmann, T. N.; Seitz, O. *J. Am. Chem. Soc.* **2006**, *128*, 15596–15597. (c) Sando, S.; Sasaki, T.; Kanatani, K.; Aoyama, Y. *J. Am. Chem. Soc.* **2003**, *125*, 15720–15721, Cai, J.; Li, X. (d) Yue, X.; Taylor, J. S. *J. Am. Chem. Soc.* **2004**, *126*, 16324–16325. (e) Willner, I.; Shlyahovsky, B.; Zayats, M.; Willner, B. *Chem. Soc. Rev.* **2008**, *37*, 1153–1165. (f) Storhoff, J. J.; Elghanian, R.; Mucic, R. C.; Mirkin, C. A.; Letsinger, R. L. *J. Am. Chem. Soc.* **1998**, *120*, 1959–1964.

10.1021/ja902951b CCC: $40.75

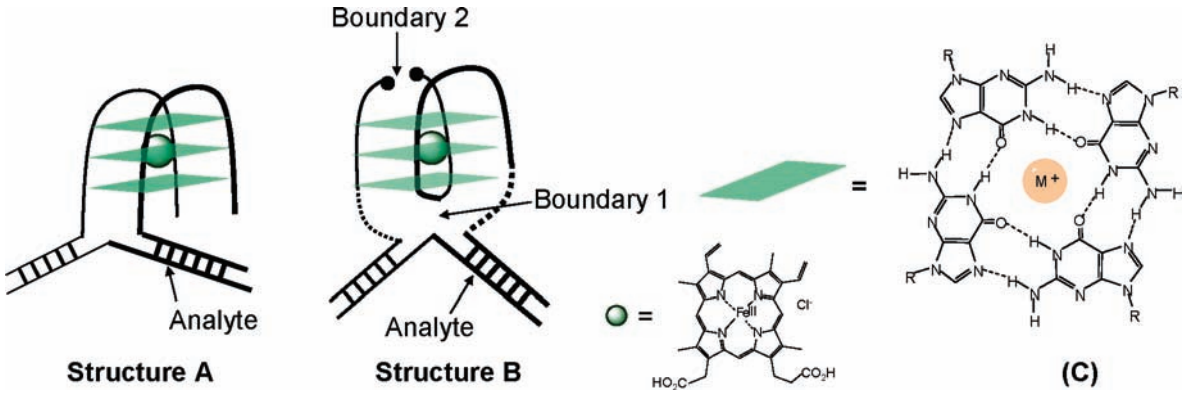

Figure 1. Reconstitution of G-quadruplex by DNA analyte; structures A and B. (C) Chemical structure of a G-quartet.

Table 1. Sequence of Oligonucleotides Used in Study

	sequence
G1	5'-GGGTAGGGCGGGTTGGG-3'
G2	5'-GGGTTTGATCTTTTGATCAAAGGGCGGGTTGGGT-3'
G3	5'-GGGTAGGGTTTGATCTTTTGATCAAAGGGTTGGGT-3'
G4	5'-GGGTAGGGCGGGTTTGATCTTTTGATCAAAGGGT-3'
G5	5'-AGGGTTAGGGTTAGGGTTAGGG-3'
G6	5'-TCTGAAGCTTTTGGGTAGGGCGGGTTGGGTTTTGCTTCAGA-3'
G7	5'-TCTGAAGCTTTTGAGTAGTTCGTGTTTGATCTTTTAAAGCCTTTTGCTTCAGA-3'
G8	5'-TCTGAAGCTTTTGGGTAGGGCGGGTTTGATCTTTTGATCAATGGGTTTTGCTTCAGA-3'
G9	5'-TCTGAAGCGGGTAGGGCGGGTTTGATCTTTTGATCAATGGGGCTTCAGA-3'
G10	5'-TCTGAAGCTTTTGGGTAGGGCGGGTTTTTTTGATCTTTTGATCAATTTTTGGGTTTTGCTTCAGA-3'
G11	5'-TCTGAAGCTTTTGGGTAGGGCGGGTTTGATCTTTTGATCAAAGGGTTTTGCTTCAGA-3'
G12	5'-TCTGAAGCTGGGTAGGGCGGGTTTGATCTTTTGATCAATGGGTGCTTCAGA-3'
G13	5'-TCTGAAGCAAAAGGGTAGGGCGGGTTTGATCTTTTGATCAATGGGAAAAGCTTCAGA-3'
G14	5'-TCTGAAGCCCCCGGGTAGGGCGGGTTTGATCTTTTGATCAATGGGCCCCGCTTCAGA-3'
T1	5'-AGAGTCCACCAAGCTTCAGATTAG-3'
T2	5'-ATCTAGAGTCCACCAAGCTTCAGATTAGAAAG-3'
T3	5'- AGAGTCCACCAACCGCTTCAGATTAG-3'
T4	5'- AGAGTCCACCAACCGCTTAAGATTAG-3'
T5	5'- AGAGTCCACCAACCGCTTTAGATTAG-3'
T6	5'- AGAGTCCACCAACCGCTTGAGATTAG-3'
Probe A1	5'-GATCAATGGGTTTTTTGGTGGACTCTAAAA-3'
Probe A2	5'-GATCAATGGGTTGGTGGACTCTAAAA-3'
Probe A3	5'-GGGTTTTTTGGTGGACTCTAAAA-3'
Probe A4	5'-GATCAATGGGTTTTTTGGTGGACTCTAGAT-3'
Probe A5	5'-GGGTTTTTTGGTGGACTCTAGAT-3'
Probe B1	5'-TCTGAAGCTTTTGGGTAGGGCGGGTTTGATC-3'
Probe B2	5'-TCTGAAGCAAAAGGGTAGGGCGGGTTTGATC-3'
Probe B3	5'-TCTGAAGCGGGTAGGGCGGGTTTGATC-3'
Probe B4	5'-TCTGAAGCTTTTGGGTAGGGCGGG-3'
Probe B5	5'-CTTTCTAATCTGAAGCTTTTGGGTAGGGCGGGTTTGATC-3'
Probe B6	5'-CTTTCTAATCTGAAGCTTTTGGGTAGGGCGGG-3'
Probe Bap	5'-TCTGAAGCTTTTGGGTAGGGCGGGTTTGA$_{AP}$TC-3'

as avidin-horseradish peroxidases conjugates.[8] The use of DNA peroxidases for biomolecule detection in homogeneous formats eliminate nonspecific binding phenomenon associated with protein-based biocatalyst, obviate the need for expensive refrigerated storage, and reduce the number of analytical steps for biomolecule sensing. So far two classes of G-rich probes, symmetric (structure **A**, Figure 1)[7b,c] and asymmetric (structure **B**, Figure 1),[7d] have been used to detect DNA analytes. Both probe designs suffer from substantial background noise (signal generated in the absence of target gene), although structure **A** somehow produces less background noise. In structure **B** (Figure 1), the sequence content of the oligonucleotides at the boundaries marked 1 and 2 would affect the topology of the reconstituted DNAzyme.[9] No comprehensive study has been undertaken to investigate the effect of the boundary architecture on the stability, topology, hemin binding, and catalysis of the reconstituted enzyme. The aims of our study were 2-fold: (a) to identify the factors that lead to the background noise associated with the use of asymmetric G-rich detection probes and (b) to discover the salient architectural features that are required to reconstitute an enzymatically proficient DNAzyme by investigating the effect that the architecture of the motifs that flank the G-quadruplex structure have on the enzymatic proficiency of the reconstituted enzyme. It was expected that information gleaned from this study would aid in the design of more sensitive

(7) (a) Xiao, Y.; Pavlov, V.; Niazov, T.; Dishon, A.; Kotler, M.; Willner, I. *J. Am. Chem. Soc.* **2004**, *126*, 7430–7431. (b) Kolpashchikov, D. M. *J. Am. Chem. Soc.* **2008**, *130*, 2934–2935. (c) Li, T.; Dong, S.; Wang, E. *Chem. Commun.* **2007**, 4209–4211. (d) Deng, M.; Zhang, D.; Zhou, Y.; Zhou, X. *J. Am. Chem. Soc.* **2008**, *130*, 13095–13102.

(8) Bonvicini, F.; Gallinella, G.; Cricca, M.; Venturoli, S.; Musiani, M.; Zerbini, M. *J. Clin. Virol.* **2004**, *30*, 134–136.

(9) (a) Cevec, M.; Plavec, J. *Biochemistry* **2005**, *44*, 15238–15246. (b) Guedin, A.; De Cian, A.; Gros, J.; Lacroix, L.; Mergny, J. L. *Biochimie* **2008**, *90*, 686–696.

colorimetric probes and would also provide some insights into how nucleic acids achieve catalysis.

Experimental Section

Materials. Normal CPGs (dA, dT, dG, and dC) and normal phosphoramidites (dA, dT, dG and dC) were purchased from Azco Biotech, Inc. Glen-Pak DNA purification cartridges were purchased from Glen Research. MOPS (3-morpholinopropanesulfonic acid), KAc (potassium acetate), and Tris-acetate were purchased from Fluka biochemika. $NaNO_3$ (sodium nitrate) was purchased from Riedel-deHaen. $MgAc_2 \cdot 4H_2O$ (magnesium acetate tetrahydrate), $ABTS^{2-}$ (2,2′-azino-bis (3-ethylbenzothiazoline-6-sulfonic acid) diammonium salt, and hemin (chloro[3,7,12,17-tetramethyl-8−13-divinylporphyrin 2,18-dipropanoato(2-)]iron(III)) were purchased from Sigma life science.

Synthesis of Oligonucleotides. All unmodified oligonucleotides were synthesized on 1 μmol scale on an Applied Biosystems (model 392) synthesizer using standard β-cyanoethylphosphoramidite-coupling protocol with DMT-on mode according to the manufacturer's manual. Deprotection and cleavage of the oligonucleotides from the CPG support were carried out by incubating the CPG powders in ammonium hydroxide for 8 h at 55 °C.

Purification of Oligonuleotides. Oligonucleotides were purified by Glen-Pak DNA purification cartridge according to the manufacturer's manual. After purification the eluent was removed in vacuo by Speedvac (Thermal Scientific, model SAVANT DNA 120), and the product was redissolved in sterile H_2O.

Determination of Yields. The oligonucleotides were quantified by UV absorbance. The optical densities were measured at 260 nm by using a quartz cuvette with a 1 cm path length on a JASCO V-630 spectrophotomer. The sample concentration was calculated by using oligo calculation at www.idtdna.com.

General Preparation of Sample before Colorimetric Measurements Assay. DNA oligomers (probes and template), water, and buffer solution consisting of Tris-acetate (20 mM), MOPS (10 mM), KAc (50 mM), $NaNO_3$ (50 mM), MgAc (10 mM), and DTT (1 μM), pH 7.9 were mixed, heated at 95 °C for 5 min, and then cooled back to room temperature for 15 min. The sample was allowed sit for 15 min on ice before a buffer solution containing hemin was added (final hemin concentration = 0.5 μM). The added hemin was allowed to complex with the DNA for 20 min. Peroxidation reactions were carried out subsequent to this complex formation.

Colorimetric Measurements Assay. The experiment was performed in a solution consisting of DNA, hemin (0.5 μM), H_2O_2 (2 mM), 2,2′-azino-bis (3-ethylbenzothiazoline-6-sulfonic acid) diammonium salt ($ABTS^{2-}$; 2 mM), in Buffers A, B, C or D: Buffer A = Tris-acetate (20 mM), MOPS (10 mM), KAc (50 mM), $NaNO_3$ (50 mM), MgAc (10 mM), DTT (1 μM), pH 7.9; Buffer B = 50 mM Tris-HCl, 50 mM KCl, pH 7.9; Buffer C = 50 mM Tris-HCl, 200 mM NaCl, pH 7.9; Buffer D = 50 mM Tris-HCl, 150 mM NH_4OAc, pH 7.9. Absorbance changes at 415 nm were monitored to characterize the rate of oxidation of $ABTS^{2-}$.

Measurement of Melting Temperature (T_m). The experiment was performed in a buffer solution consisting of Tris-acetate (20 mM), MOPS (10 mM), KAc (50 mM), $NaNO_3$ (50 mM), MgAc (10 mM), DTT (1 μM), pH 7.9 (Buffer A). The sample was covered with mineral oil. Absorbance changes at 260 nm were monitored by JASCO V-650 spectrophotomer.

Circular Dichromism Experiments (CD). CD experiments were performed on a JASCO J-810 spectropolarimeter at 25 °C in a 1 cm path length cuvette. The concentration of DNA in Buffers A, B, C or D was 5 μM. Before the measurement, the sample was heated to 95 °C, cooled to room temperature for 15 min, and cooled on ice for 2 h. CD measurements from 220 to 350 nm were taken. The data pitch was 1 nm. The scan speed was 50 nm/min. The response was 8 s. The bandwidth was 1 nm. Each spectra was corrected by subtracting the CD of the buffer. For CD measurements of DNA-hemin complexes, hemin concentration was 12.5 μM. DNA-hemin complexation was done for 2 h at room temperature before CD measurements were taken.

Calculation of Binding Constants. The saturation curve for the complexing of hemin to DNA was determined by plotting absorbance changes in the Soret band (404 nm) as a function of DNA concentration. The dissociation constant (K_d) was obtained by fitting the saturation plot with the following equation described by Wang et al.[10]

$$[\mathrm{DNA}]_0 = K_d(A - A_0)/(A_\infty - A) + [P_0](A - A_0)/(A_\infty - A_0)$$

where $[\mathrm{DNA}]_0$ is the initial concentration of DNA; $[P_0]$ is the initial concentration of monomeric hemin (The hemin concentration was calculated using ε_{398}: 80000 M^{-1} cm^{-1}); A_∞, and A_0 represent hemin absorbance at saturating DNA concentrations and in the absence of DNA.

pK_a Determination. The various buffers used were: pH 3.0−5.2 (acetate buffer), pH 6.0−6.9 (phosphate buffer), pH 7.2−8.5 (Tris-HCl buffer), pH 9.0−10.5 (glycin-NaOH buffer). All buffer solutions contained 50 mM KCl to ensure proper DNA folding. The reactions were carried out at 20 °C in buffers at different pH values. All buffers also contained 0.05% Triton X-100.

Fluorescence Measurement of 2-Aminopurine. Fluorescence studies were performed on a Cary Eclipse Fluorescence spectrophotometer. The instrument settings were chosen as follows: λ_{ex} = 303 nm (slit 5 nm), λ_{em} = 310−600 nm (slit 5 nm), the response was 2 s. The measurements were carried out at 20 °C in Buffer A. The DNA concentration was 3 μM. Before the measurement, the sample was heated up to 95 °C for 5 min, cooled to room temperature for 15 min, and then further cooled on ice for 2 h.

Scheme 1. Duplex-Assisted G-Quadruplex Reassembly

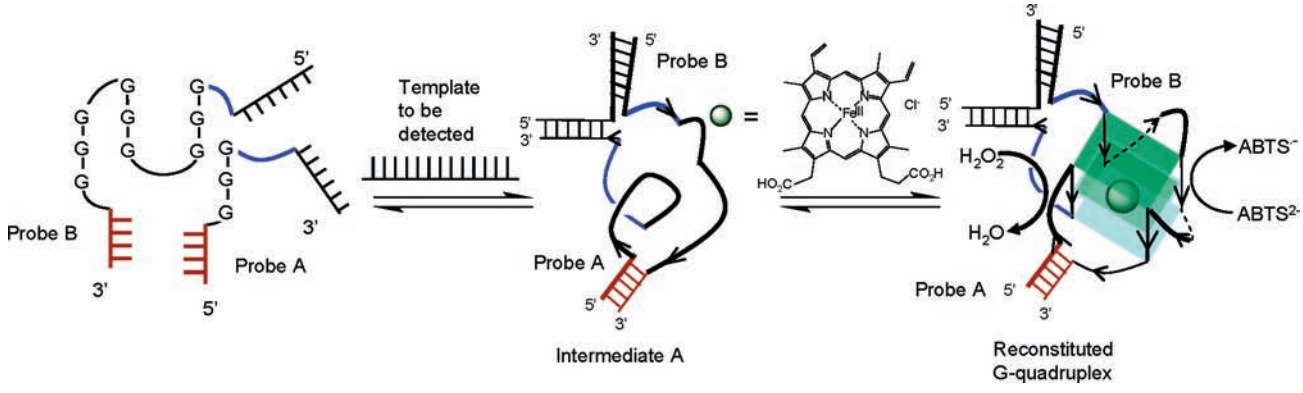

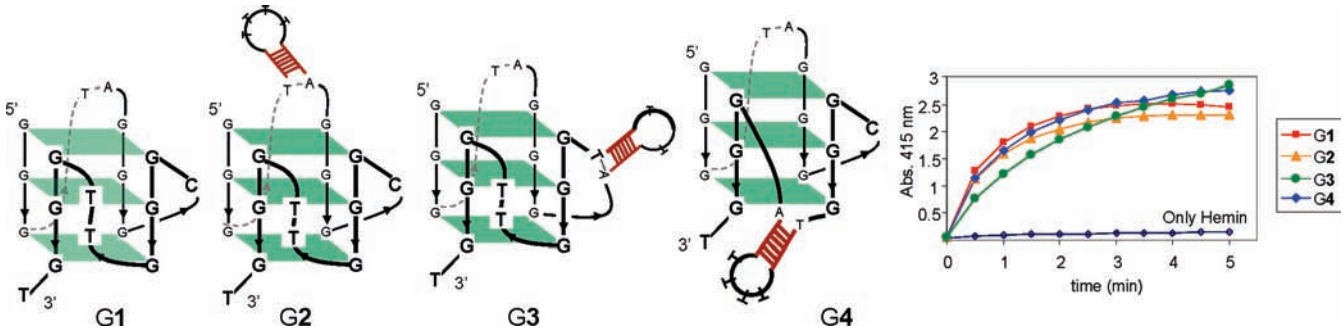

Figure 2. Peroxidase-mimicking DNAzyme activities of G-quadruplexes. G**2**-G**4** have one of the loops extended into a duplex structure. The peroxidation reaction involved the oxidation of $ABTS^{2-}$ into $ABTS^{1-}$ by the DNAzymes. The concentration of the oxidized product, $ABTS^{1-}$ is proportional to the absorbance at 415 nm. All reactions were done in Buffer A.

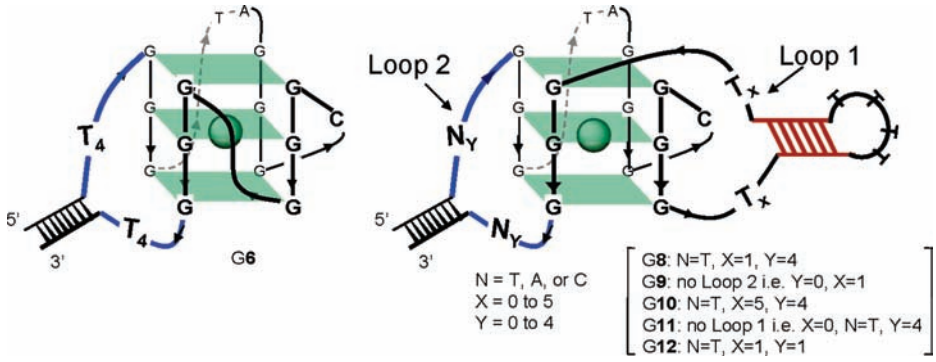

Figure 3. Parallel form of the G-quadruplex.

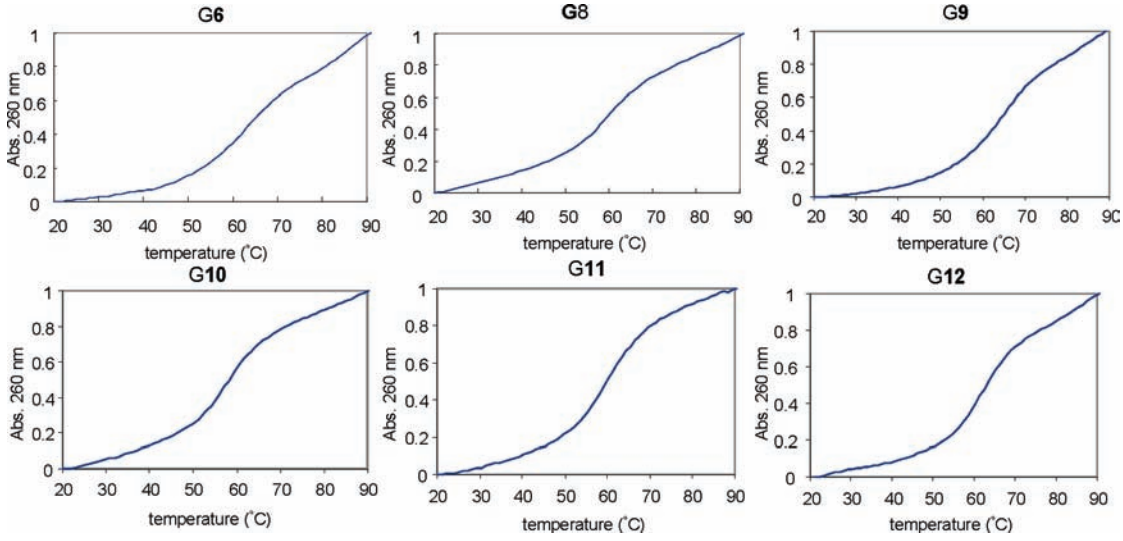

Figure 4. Melting profiles of various intramolecular G-quadruplexes. The oligonucleotides, 1 μM in buffer A, were first heated to 95 °C and slowly cooled to 4 °C overnight before the melting experiments were done. All experiments were monitored at 260 nm, and the samples were heated at a rate of 1 °C/min. The *y*-axis shows the normalized relative absorbance.

The sample was incubated at 20 °C for 5 min before fluorescence measurements were taken.

Results and Discussion

G-quadruplex formation is a step-by-step process involving several topological intermediates. During the folding process to reconstitute a peroxidase-mimicking DNAzyme, a significant fraction of the folding molecules can become kinetically trapped in conformations that are poor peroxidase enzymes. Currently it is unknown which of the many G-quadruplex conformations (parallel, antiparallel or mixed types) is/are the most efficient peroxidase mimicking enzymes. It is also unknown if there is a correlation between G-quadruplex thermal stability and

Table 2. T_m Values for Melting of G-Quadruplexes That Have One of the Loops Extended into a Duplex Structure

	T_m (260 nm) (°C)
G**6**	63.0
G**8**	59.0
G**9**	65.1
G**10**	57.1
G**11**	61.3
G**12**	61.4

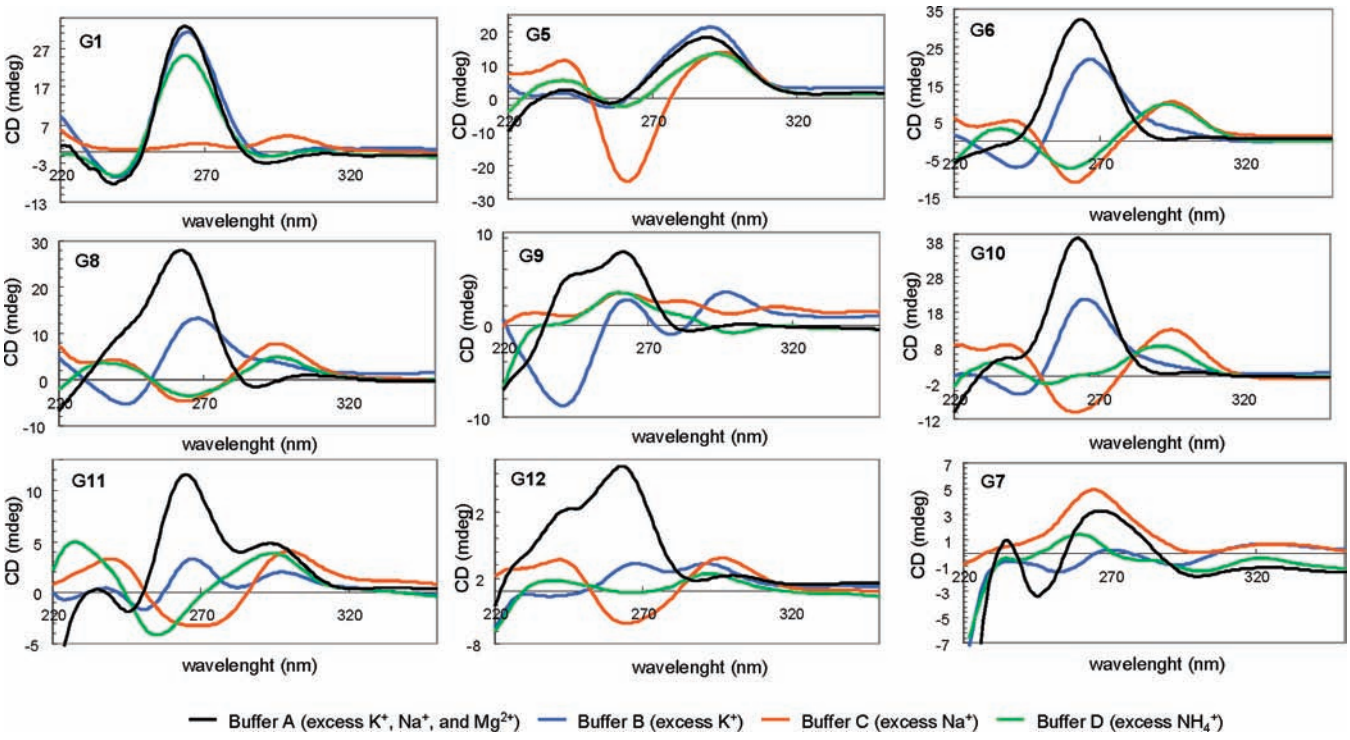

Figure 5. Circular dichroism (CD) spectra of G-quadruplexes that have one of the loops extended into a duplex structure. G**7** is a control oligonucleotide that cannot form intramolecular G-quadruplex.

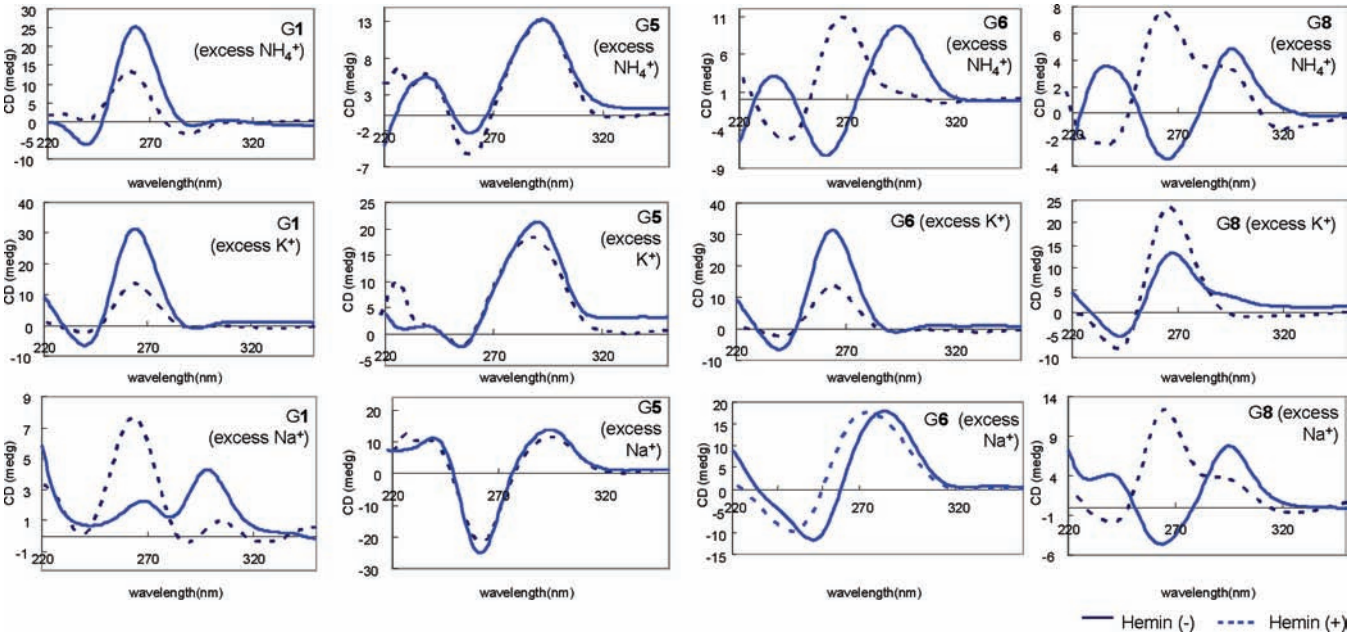

Figure 6. CD spectra of G-quadruplexes in the presence (dashed blue line) and absence (solid blue line) of hemin. The addition of hemin to the G-quadruplexes caused a blue shift in the CD spectra.

enzymatic proficiency. In order to arrive at catalytically proficient reconstituted G-quadruplex DNAzymes for biomolecule sensing, it is imperative that one knows how a particular probe design affects the topology and stability of the reconstituted G-quadruplex and also how topology and stability of the enzyme influence the catalytic activities of the reconstituted enzymes. We rationalized that two probes that have free "non-sticky" ends will have many accessible folding landscapes, hence would have a higher propensity to become trapped into kinetically irreversible states. Therefore, strategies that constrain

Table 3. Absorption Parameters of Hemin/DNAzyme and Hemin/Protein Complexes

	Soret		E band	D band		
	(nm)	ε_M	(nm)	(nm)	ε_M	spin/coord.
G**1**	403	1.45×10^5	498	622	0.77×10^4	HS/6C
G**8**	402	1.47×10^5	504	622	0.86×10^4	HS/6C
heme-ox*	404	1.65×10^5	500	631	1.10×10^4	HS/6C
Met Hb*	405	1.79×10^5	500	631	0.44×10^4	HS/6C

* Quoted values are from refs 23 and. 25.

Scheme 2. Ligand Exchange and Oxidation of Iron Center in Hemin

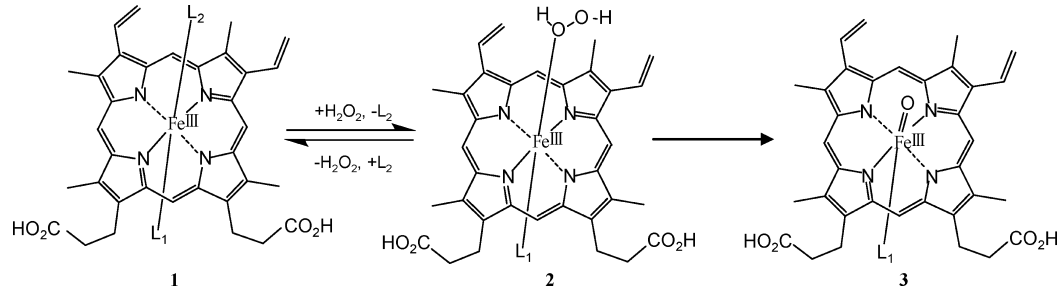

Table 4. p*K*a Values for the Acid/Alkaline Transitions of Hemin/DNA and Hemin/Protein Complexes

	pK_a
G**1**	8.30 ± 0.18
G**5**	5.45 ± 0. 29
G**6**	8.54 ± 0.10
G**8**	8.46 ± 0.14
G**9**	8.57 ± 0.33
G**10**	8.39 ± 0. 52
G**11**	7.96 ± 0. 13
G**12**	8.56 ± 0. 17
Met Hem[a]	8.33 ± 0. 02
PS2.M[a]	8.70 ± 0. 03
HRP[a]	10.9 ± 0. 40

[a] Quoted values are from ref 23.

the ends of the two G-rich probes which reconstitute into an active G-quadruplex DNAzyme should lead to a better folded enzyme. The caveat is that such a strategy could also lead to high background signal because the two separate probes can associate and fold into active DNAzymes in the absence of a DNA analyte.

Endowing the Separate Split G-Quadruplex DNAzyme Probes with Limited Complementary Sequences. TeHyP (an acronym for **T**emplate **e**nhanced **Hy**bridization **P**rocesses) encompasses a detection strategy whereby two probes that have complementary sequences but cannot form a duplex at ambient temperatures (20−30 °C) can be made to hybridize to each other in the presence of an analyte that binds to both probes in a juxtaposed manner. The resulting duplex structure then acts as a platform for further processing that leads to the generation of a measurable signal. For example in the junction probe technology that was recently reported by us, when the two TeHyP probes anneal to each other in the presence of a template, a duplex region that contains a restriction site is formed. Cleavage of the resulting restriction site by a restriction endonuclease results in the generation of a fluorescent signal and a signal amplification cascade.[11] We reasoned that, similar to our junction probes technology, split G-quadruplex probes that were endowed with complementary Watson−Crick sequences of seven or less base pairs would have a low propensity to reassemble at ambient temperature but would efficiently reassemble into active peroxidase-mimicking enzymes in the presence of analytes that bind the two probes in a juxtaposed manner; in this instance the duplex region (colored brown in Scheme 1) which has a faster folding kinetics[12] would form first (see intermediate A, Scheme 1) and then cooperatively aid the G-quadruplex folding.

Because the strategy outlined in Scheme 1 has replaced one of the G-quadruplex loops with a duplex (colored brown), we first investigated if any of the loops of a prototypical G-quadruplex DNAzyme, G**1** (Figure 2), could be replaced with a duplex without diminishing G**1**'s peroxidase activity. The DNAzyme G**1** belongs to the 2-1-2 group of sequences. For the purpose of this paper we designate G-quadruplexes G**2**, G**3** and G**4** (Figure 2) as belonging to the $D_{x\text{-}y\text{-}z}$-1-2, 2-$D_{x\text{-}y\text{-}z}$-2 and 2-1-$D_{x\text{-}y\text{-}z}$ groups respectively. $D_{x\text{-}y\text{-}z}$ denotes an intervening stem−loop structure between contiguous guanines; x = number of mismatched base pairs immediately next to the G-tetrad, y = number of matched base pairs in the stem region and z = number of bases in the loop section. Using this nomenclature, G**2** is designated as $D_{0\text{-}7\text{-}4}$-1-2, G**3** is designated as 2-$D_{0\text{-}7\text{-}4}$-2 and G**4** is designated as 2-1-$D_{0\text{-}7\text{-}4}$. In the presence of hemin and hydrogen peroxide, G**1**, G**2**, G**3** and G**4** oxidized the chromogenic substrate 2,2′-azino-bis(3-ethylbenzthiazoline-6-sulfonic acid) diammonium salt ($ABTS^{2-}$) into $ABTS^{1-}$ (Figure 2) at similar rates; giving us the impetus to embark on re-engineering G**1** into a duplex-assisted G-quadruplex.

Recently, Dong has also shown that when a duplex is placed next to the floors of the G-tetrad, the folding of the G-quadruplex structure is enhanced.[12] It must be noted however, that our approach which places the duplex moiety in the loop region is conceptually different from Dong's approach that placed the duplex region at the base of the G-quadruplex; thereby maintaining the conventional single stranded loops in the resulting G-quadruplex.[12] Our study is therefore the first to investigate the effect of replacing the single stranded loop regions of G-quadruplexes with duplex structures on DNAzyme catalysis.

G-quadruplex topologies are determined by several factors such as type of cations present,[13] the composition of the loops[14] and the number of stacked G-tetrads.[15] For example, it has been observed that a single base change in the loop of human and *Tetrahymena* telomeric repeat affects both the folding and stability of the G-quadruplex.[16] Loop−loop stacking and hydrogen-bonding interactions have also been shown to influence quadruplex topologies.[17] Therefore, we investigated how the sequence context of the loops that connect the G-tracts and the

(10) Wang, Y.; Hamasaki, K.; Rando, R. R. *Biochemistry* **1997**, *36*, 768–779.
(11) Nakayama, S.; Lei Yan, L.; Sintim, H. O. *J. Am. Chem. Soc.* **2008**, *130*, 12560–12561.
(12) Li, T.; Wang, E.; Dong, S. *Chem. Eur. J.,* **2009**, *15*, 2059–2063.
(13) Sen, D.; Gilbert, W. *Nature* **1990**, *344*, 410–414.
(14) (a) Luu, K. N.; Phan, A. T.; Kuryavyi, V.; Lacroix, L.; Patel, D. J. *J. Am. Chem. Soc.* **2006**, *128*, 9963–9970. (b) Rachwal, P. A.; Brown, T.; Fox, K. R. *FEBS Lett.* **2007**, *581*, 1657–1660. (c) Bugaut, A.; Balasubramanian, S. *Biochemistry* **2008**, *47*, 689–697.
(15) Rachwal, P. A.; Brown, T.; Fox, K. R. *Biochemistry* **2007**, *46*, 3036–3044.
(16) Miyoshi, D.; Karimata, H.; Sugimoto, N. *Angew. Chem., Int. Ed.* **2005**, *44*, 3740–3744.
(17) (a) Keniry, M. A.; Owen, E. A.; Shafer, R. H. *Nucleic Acids Res.* **1997**, *25*, 4389–4392. (b) Smirnov, I.; Shafer, R. H. *Biochemistry* **2000**, *39*, 1462–1468. (c) Risitano, A.; Fox, K. R. *Biochemistry* **2003**, *42*, 6507–6513.

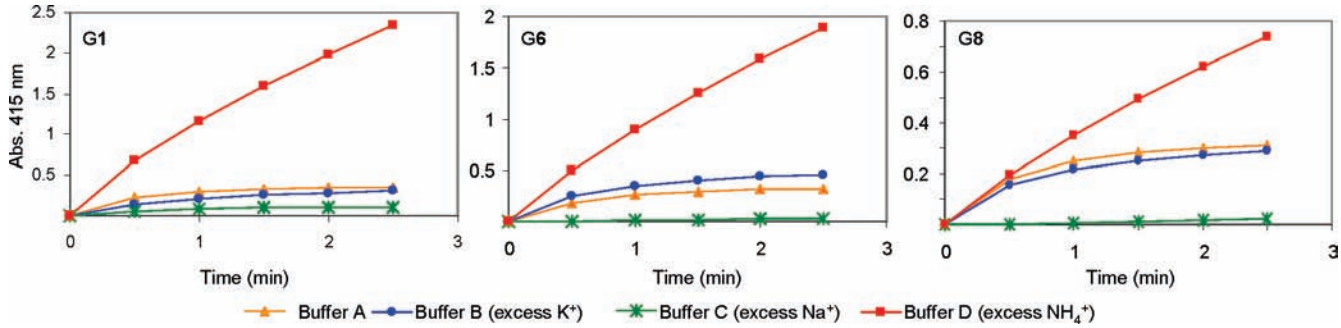

Figure 7. Effect of monovalent cation on the speed of the DNAzyme-catalyzed peroxidase reaction. The *y*-axis represents the absorbance of the peroxidation product ($ABTS^{1-}$).

Table 5. Effect of Various Monovalent Cations on the Dissociation Constants of Hemin/DNAzyme Complexes, Initial Speed of the DNAzyme-Catalyzed Peroxidation Reaction and Speed of Reaction after 5 min, Proportion of Active DNAzyme Remaining after 5 min (*V*2/*V*1) and Turnover Numbers (TON) of Peroxidase-Mimicking DNAzymes

	buffer	K_d	$V1_{t=0}$ (μM/min)[a]	$V2_{t=5}$ (μM/min)[a]	*V*2/*V*1 (%)	TONs
G1	Buffer A	0.73 ± 0.14	196.2	0.0	0.0	90
	Buffer B (K^+)	1.47 ± 0.48	117.7	0.5	0.4	97
	Buffer C (Na^+)	–	48.3	1.9	4.0	38
	Buffer D (NH_{4+})	0.13 ± 0.05	362.4	125.3	34.6	1393
G6	Buffer A	0.42 ± 0.04	186.2	0.0	0.0	90
	Buffer B (K^+)	0.84 ± 0.27	197.7	0.0	0.0	131
	Buffer C (Na^+)	–	–	–	–	–
	Buffer D (NH_{4+})	0.64 ± 0.13	261.9	126.7	48.4	1097
G8	Buffer A	0.40 ± 0.01	160.8	1.1	0.7	91
	Buffer B (K^+)	1.30 ± 0.18	128.2	0.0	0.0	87
	Buffer C (Na^+)	–	–	–	–	–
	Buffer D (NH_{4+})	0.75 ± 0.15	108.9	39.9	36.7	565

[a] V = the velocity of reaction catalyzed by 1 μM DNAzyme; $V = d[ABTS^*]/dt = dA/dt \times (1/\varepsilon L) \times (10^{-6}/[DNA])$. Where [ABTS*] = concentration of oxidized ABTS, A = absorbance, ε = molar absorptivity: $\varepsilon(ABTS) = 3.6 \times 10^4$ L mol^{-1} cm^{-1}, L = path length (cm), [DNA] = concentration of DNAzyme. The following equations were used to calculate dA/dt for peroxidation reactions in Buffer D (see Supporting Information Figures S5−14 for the determination of dA/dt equations; G**1**: Buffer D: $dA/dt = (-6 \times 10^{-7}t^5) + (40 \times 10^{-6}t^4) - (8 \times 10^{-4}t^3) + (8.7 \times 10^{-3}t^2) - (0.0452t) + 0.1305$ [for $t = 0-5$ min]. G**6**: Buffer D: $dA/dt = (-42 \times 10^{-8}t^5) + (25 \times 10^{-6}t^4) - (4 \times 10^{-4}t^3) + (5.4 \times 10^{-3}t^2) - (0.0296t) + 0.0943$ [for $t = 0-5$ min]. G**8**: Buffer D: $dA/dt = (-24 \times 10^{-9}t^5) + (20 \times 10^{-7}t^4) - (8 \times 10^{-5}t^3) + (12 \times 10^{-4}t^2) - (0.0092t) + 0.0392$ [for $t = 0-5$ min]. Units of $K_d = \mu$M.

Table 6. Dissociation Constants of Hemin/DNAzyme complexes and initial velocities of the DNAzyme-catalyzed peroxidation reactions in Buffer A (containing K^+, Na^+ and Mg^{2+})

	buffer	K_d	$V_{t=0}$ (μM/min)[a]
G**8**	Buffer A	0.40 ± 0.01	160.8
G**9**	Buffer A	1.01 ± 0.04	58.9
G**10**	Buffer A	0.39 ± 0.11	186.2
G**11**	Buffer A	0.30 ± 0.08	150.9
G**12**	Buffer A	0.51 ± 0.26	116.7

[a] V: velocity of the reaction catalyzed by 1 μM DNAzyme. Calculation of $V_{t=0}$; same as Table 5 (see Supporting Information, Figures S15−21). Units of $K_d = \mu$M.

duplex regions (see loops 1 and 2, Figure 3) affect the stability, G-quadruplex conformation (parallel, antiparallel or hybrid structures), hemin-binding and the enzymatic activities of the peroxidase-mimicking enzymes.

Some of the unanswered questions regarding how the properties of DNAzymes affect enzymatic proficiency are: (a) Are more stable DNAzymes (stability was qualitatively measured via thermal melting experiments, *vide infra*) better enzymes than less stable oligonucleotides? (b) Does hemin (the cofactor for the peroxidation reaction) have a binding preference for any particular G-quadruplex topology?

Thermal Melting Experiments. The thermal denaturation of the G-quadruplexes that have a general structure as shown in Figure 3, (G**6**, G**8**-G**12**) resulted in a hyperchromism at 260 nm (Figure 4). The melting profiles did not change with strand concentration; indicating that monomeric intramolecularly folded species were the predominant species present in solution. The differentiated melting curves for G**6**, G**8**-G**12** mainly showed one resolved peak (see Supporting Information Figure S1). This suggests that either the melting temperatures of the duplex and G-quadruplex regions are similar or the melting processes of the two domains are cooperative. When the canonical Watson−Crick duplex between the two G-tracts melts, an 18-nucleotide loop will be formed. In most cases, G-quadruplexes with longer loops tend to form antiparallel structures and are less stable than those with shorter loops.[18]

Circular Dichromism Experiments. The folding topology of G-quadruplexes can be deduced from specific signatures in their circular dichromism (CD) spectra.[19] Positive CD signals around 295 and 247 nm and a negative signal around 265 nm are characteristics of an antiparallel conformer,[20] whereas a positive CD signal at 263 nm and a negative CD signal at 240 nm are characteristics of a parallel conformer.[21] A CD spectrum that shows strong positive signals at both 265 and 295 nm or a positive signal at 265 nm and a shoulder at 295 nm is indicative of either a mixed hybrid-type structure or a mixture that contains both parallel and antiparallel conformers. The oligonucleotides G**8**, G**9** and G**12** belong to the 2-1-D_{1-6-4} group and mainly differ by virtue of the number of nucleotides in loop 2. G**8** has eight thymidine nucleotides in loop 2, whereas G**12** has two thymidine nucleotides and G**9** has no loop 2; in G**9**, the G-quadruplex structure is directly appended to a duplex region. Difference CD spectra[22] of G**8**, G**9** and G**12** have different signatures;

(18) (a) Hazel, P.; Huppert, J.; Balasubramanian, S.; Neidle, S. *J. Am. Chem. Soc.* **2004**, *126*, 16405–16415. (b) Smirnov, I.; Shafer, R. H. *Biochemistry* **2000**, *39*, 1462–1468. (c) Smargiasso, N.; Rosu, F.; Hsia, W.; Colson, P.; Baker, E. S.; Bowers, M. T.; De Pauw, E.; Gabelica, V. *J. Am. Chem. Soc.* **2008**, *130*, 10208–10216.
(19) There is still some debate on the use of CD to determine G-quadruplex topologies, see: Lane A. N. , ChairesJ. B., Gray R. D. Trent J. O., Nucleic Acids Res. 2008, *36*, 5482−5515.
(20) (a) Wang, Y.; Patel, D. J. *Structure* **1993**, *1*, 263. (b) Ambrus, A.; Chen, D.; Dai, J.; Bialis, T; Jones, R. A.; Yang, D. *Nucleic Acids Res.* **2006**, *34*, 2723–2735.
(21) Jin, R.; Gaffney, B. L.; Wang, C.; Jones, R. A.; Breslauer, K. J. *Proc. Natl. Acad. Sci. U.S.A.* **1992**, *89*, 8832–8836.
(22) Difference CD spectra were obtained by subtracting the CD spectra of the oligonucleotides in a buffer lacking the monovalent cations K(I), Na(I) or NH_4(I) from that which contained K(I), Na(I) or NH_4(I).

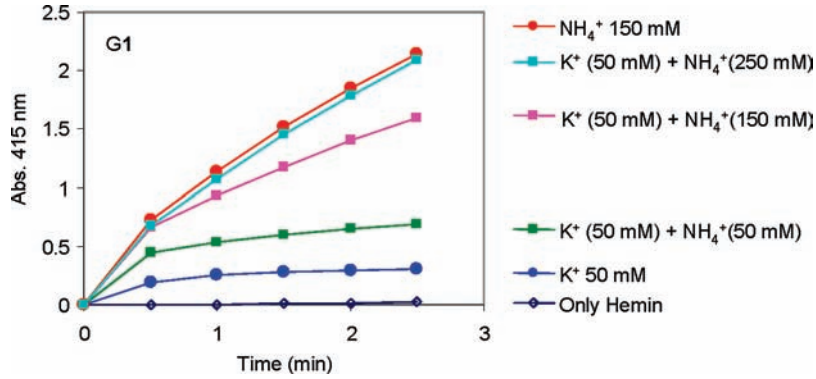

Figure 8. Effect of increasing concentration of ammonium ion on catalyst inactivation. The *y*-axis represents the absorbance of the peroxidation product ($ABTS^{1-}$).

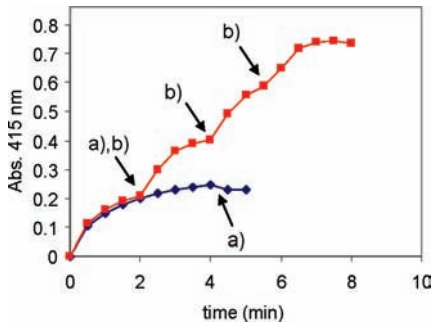

Figure 9. Addition of fresh DNAzyme (G**1**) or H_2O_2 to stalled peroxidase reaction; (a) addition of H_2O_2 and (b) addition of G**1**. The *y*-axis represents the absorbance of the peroxidation product ($ABTS^{1-}$).

implying that the architecture of the domain that immediately precedes the quadruplex structure (loop 2 in our case) influences the G-quadruplex topology. For example, G**8** only differs from G**12** by virtue of the number of nucleotides in loop 2, yet G**8** exists predominantly as an antiparallel conformer in Buffer D (excess NH_4^+) and parallel conformer in Buffer B (excess K^+), whereas G**12** exists as a hybrid or a mixture of parallel and antiparallel structures in both Buffers B and D (see Figure 5). Both G**1** and G**6** belong to the 2-1-2 group; however, the 5′- and 3′-ends of G**6** are tied together via duplex formation, whereas the ends of G**1** are not constrained. Interestingly, despite the fact that both G**1** and G**6** belong to the same quadruplex sequence group 2-1-2 they form different G-quadruplex conformers (see Figure 5). G**6** exists as an antiparallel structure in both Buffer D (excess NH_4^+) and C (excess Na^+), whereas G**1** exists as a hybrid-type or a mixture of parallel/antiparallel conformers in the aforementioned buffers. Loop 1 (see Figure 3) also influences the conformer distribution of the G-quadruplexes. G**8**, G**10** and G**11** only differ from each other by virtue of the number of thymidine nucleotides in loop 1 (G**11**, G**8** and G**10** have 0, 2, and 8 thymidine nucleotides in loop 1 respectively). The CD spectra of G**11** are significantly different from that of G**8** and G**10** in Buffers A, B and C. In the presence of excess Na^+, the conformations of all of the G-quadruplexes that belong to the 3−3−3 (G**5**) or 2-1-$D_{x\text{-}y\text{-}z}$ groups, with the exception of G**9**, are antiparallel. Interestingly, although oligonucleotides G**1** and G**6** both belong to the 2-1-2 group, G**1** (which has free 3′- and 5′-ends) does not form the antiparallel conformer in a buffer that contains excess Na^+ whereas G**6** (which has constrained 3′- and 5′-ends) forms an antiparallel G-quadruplex conformation in the presence of excess Na^+. The difference CD spectrum of G**7** (a control oligonucleotide which lacks G-tract sequences hence can not form a quadruplex structure) does not show peaks that correspond to the typical G-quadruplex signature peaks seen in the other G-tract containing sequences.

Hemin Binding to G-quadruplexes (UV Titrations and CD). As already mentioned, hemin acts as a cofactor for the G-quadruplex-catalyzed peroxidase reaction. Although it has been shown that many aromatic ligands bind to G-quadruplexes in an end-capping mode,[23] the site of hemin binding (intercalation or end-capping) to peroxidase-mimicking G-quadruplexes has been a subject of debate.[24] It has not been unambiguously demonstrated which of the G-quadruplex conformers (parallel, antiparallel or mixed type) has the highest affinity for hemin. We investigated via CD if hemin binding to G**1**, G**5**, G**6** and G**8** shifted the G-quadruplex conformer distribution to any one particular topology. Addition of hemin to G**5** in Buffers B, C and D (excess K^+, Na^+ and NH_4^+, respectively) did not lead to any significant changes in the CD spectra of G**5** (see Figure 6). This was consistent with our earlier observation that hemin did not bind to G**5** because the addition of G**5** to hemin did not cause a significant change in hemin's molar absorptivity (see Supporting Information Figure S4, G**5**). Addition of hemin to G**1**, G**6** or G**8** did, however, cause significant changes in their respective CD signatures; there was a reduction of the CD band centered at 295 nm and an increase in the band centered around 265 nm. The changes were most significant in buffers that contained excess NH_4^+ cations (see Figure 6, CD spectra for G**5** and G**8**); addition of hemin to antiparallel G-quadruplex conformers in buffers that contained excess NH_4^+ lead to a quadruplex conformational switch to parallel/mixed-type structures. In the absence of other structural data such as NMR or X-ray crystals, it is impossible to determine if the hemin/DNAzyme complex has a parallel or mixed-type topology.

Does the Size of Loop 1 or 2 in DNAzymes Shown in Figure 3 Influence Ligand Exchange and Chemistry at the Active Site? The mechanism that is utilized by hemin-binding peroxidase-mimicking nucleic acid catalysts to oxidize organic molecules has not been completely deciphered. However, circumstantial evidence indicates that nucleic acid peroxidases catalyze oxidation reactions via mechanisms that are similar to those used by horseradish peroxidase (HRP) and other heme

(23) Gabelica, V.; Baker, E. S.; Teulade-Fichou, M. P.; De Pauw, E.; Bowers, M. T. *J. Am. Chem. Soc.* **2007**, *129*, 895–904.
(24) Lee, H. W.; Chinnapen, D. J. F.; Sen, D. *Pure Appl. Chem.* **2004**, *76*, 1537–1545.

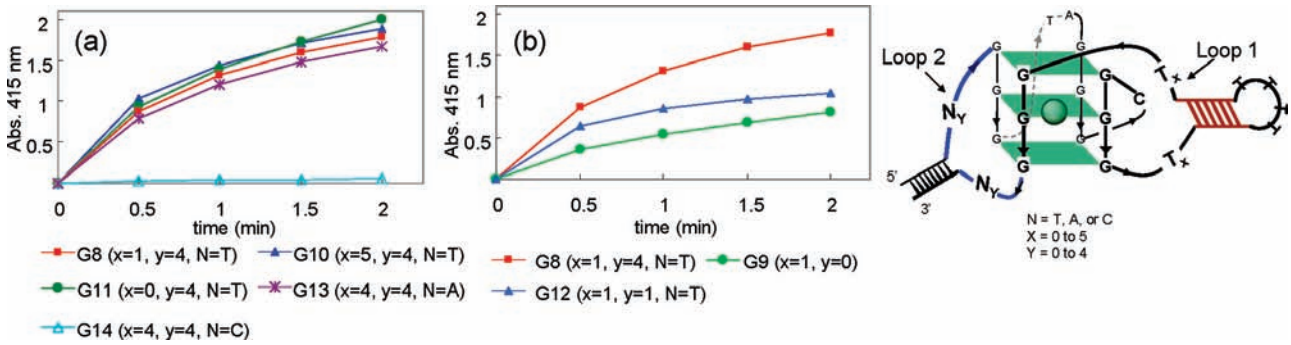

Figure 10. (a) Effect of size and content of loop 1 on peroxidase reaction. (b) Effect of size of loop 2 on peroxidase reaction. *y*-axis represents the absorbance of the peroxidation product ($ABTS^{1-}$).

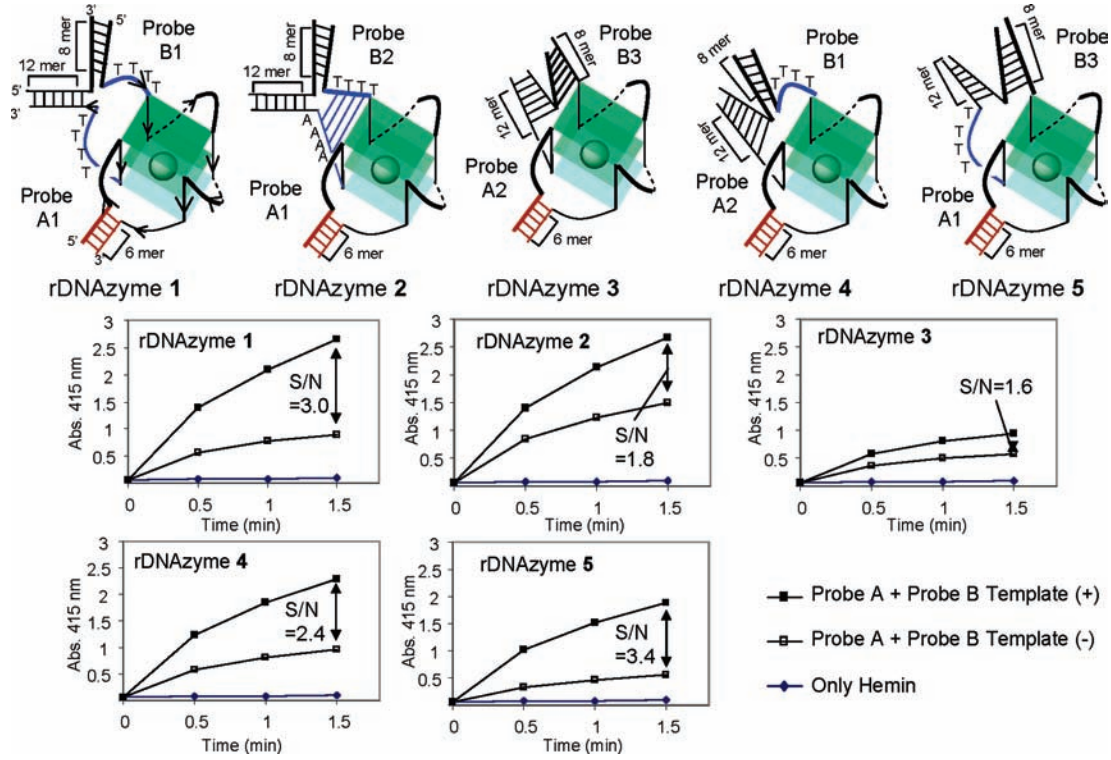

Figure 11. Detection of DNA analytes by TeHyP split G-quadruplex probes. rDNAzymes **1**-**5** are reconstituted by adding the split G-quadruplex probes to a template that binds the two probes in a juxtapose manner, see Scheme 1. The *y*-axis represents the absorbance of the peroxidation product ($ABTS^{1-}$). S/*N* = signal-to-noise ratio; which is the ratio of the absorbance of the peroxidation product, $ABTS^{-1}$, produced by DNAzymes that are formed by probes and DNA analyte and that of DNAzymes that are reconstituted in the absence of DNA analyte (i.e., probe A and probe B without adding template).

proteins such as methemoglobin and metmyoglobin.[25] It has been demonstrated via UV−vis and electron paramagnetic resonance (EPR) spectroscopies that the electronic character of the hemin iron, after complexation to G-quadruplexes, closely resemble those of heme proteins.[26] The soret bands, E and D bands of hemin when bound to DNAzymes such as PS5.M and the ones used in our study (G**1** and G**8**) have similar values compared to those of the bands observed in other heme proteins (see Table 3). The red shift for the soret bands of G**1** and G**8** implies that hemin binds to a hydrophobic pocket in these DNAzymes. The E and D bands at ∼500 and 622 nm for hemin bound to both G**1** and G**8** are indicative of a high-spin six-coordinate iron center.

For six-coordinate hemin iron centers, water can bind as the axial ligand (Scheme 2). The peroxidation reaction is done at basic pH (∼8.0), and the degree of ionization of the water molecule that is coordinated to the axial position of the hemin iron affects the catalytic efficiency of the peroxidase-mimicking oligonucleotides.

For example the pK_a of the hemin-bound water in G**5** (an oligonucleotide which has a poor peroxidase activity) is 5.45 (Table 4) whereas the pKas of the hemin-bound water in the oligonucleotides that showed enhanced peroxidase activities (G**1**, G**6**, G**8**-G**12**) were generally greater than 8.0 (Table 4 and Supporting Information, Figure S2). The low pK_a of the hemin-bound water in G**5** implies that at the reaction pH of 8.0, the majority of the hemin metal centers in G**5** are ligated with hydroxide ion at the axial position. Because the hydroxide ion

(25) Travascio, P.; Sen, D.; Bennet, A. J. *Can. J. Chem.* **2006**, *84*, 613–619.
(26) (a) Travascio, P.; Li, Y.; Sen, D. *Chem. Biol.* **1998**, *5*, 505–517. (b) Bruice, T. C. In *Mechanistic principles of enzyme activity*; Liebman, J. F.; Greenberg, A., Eds.; VCH Publishers: Deerfield Beach, FL, 1988; Vol. 9, pp 227−277.

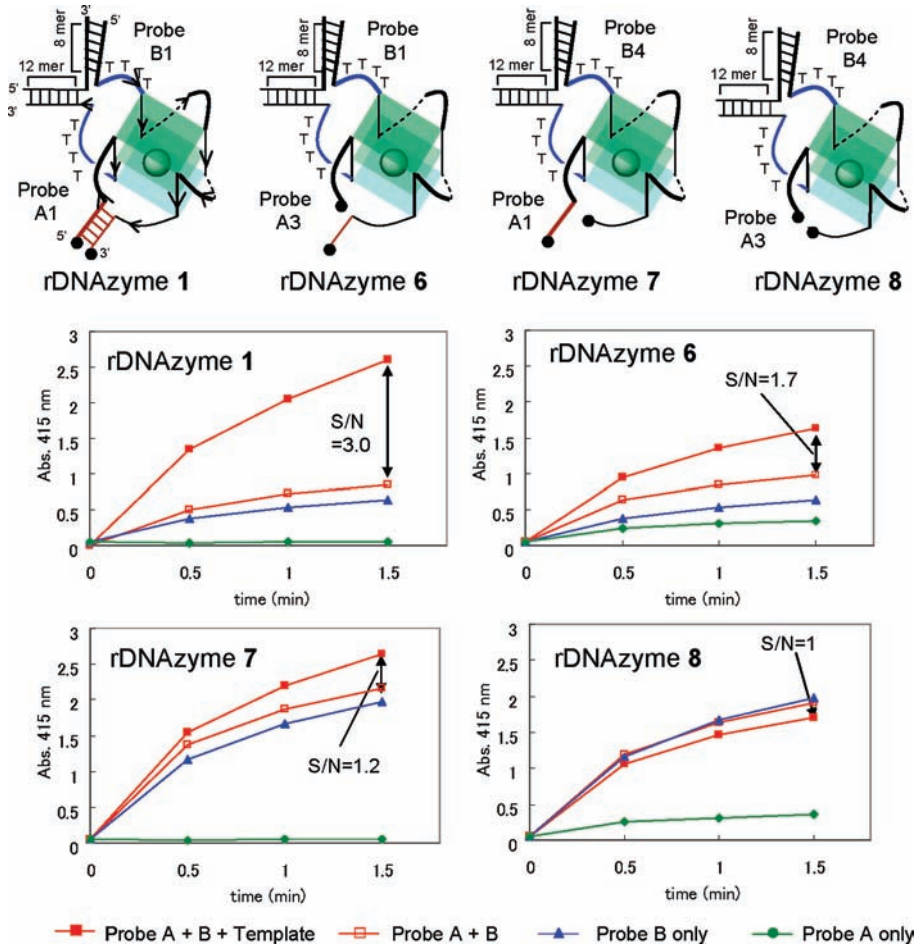

Figure 12. Time course measurement of absorbance of peroxidation product, $ABTS^{1-}$ in the presence of tripartite rDNAzymes **1**, **6**−**8**, separate probes (A and B) and combination of probes A and B without a DNA analyte. Probes that have limited regions of complementarity (see rDNAzyme **1**) can distinguish between the presence and absence of DNA analytes most sensitively (i.e., rDNAzyme **1** has the highest *S/N* ratio at time = 1.5 min).

is more difficult to displace than water, the formation of an outer-sphere porphyrin/hydrogen peroxide complex (an important intermediate in the postulated catalytic cycle) will be disfavored in G**5**.

Effect of Monovalent Cation on DNAzyme Catalysis. It is well documented that cations influence the topology of G-quadruplexes.[13,27] Should the different G-quadruplex conformers oxidize ABTS at different rates then, it follows that cations will have an indirect effect on enzymatic proficiency by favoring a particular G-quadruplex conformer. Additionally, cations will have an indirect effect on DNAzyme catalysis if the dissociation constant of the hemin/DNAzyme complex depends on the quadruplex topology. We first investigated if the tightness of the binding between hemin and the DNAzymes correlated with enzymatic proficiency. The dissociation constants for the hemin/DNAzyme complexes varied with the type of monovalent cation that was in excess (see Tables 5 and 6 and Supporting Information Figure S3 and S4). In general, the hemin/DNAzyme complexes were more stable in buffers containing excess ammonium cations than those containing excess potassium or sodium cations (see Figure 7, Table 5; K_d's for G**1**, G**6** and G**8**). G**6** and G**8** exist as antiparallel conformers in buffers containing excess ammonium, whereas they exist predominantly as parallel or mixed type in buffers containing excess potassium. It is therefore counterintuitive that the stability of hemin/DNAzyme complex in buffers containing excess ammonium is higher than in those containing excess potassium. However, it has been demonstrated by others[28] and also by this study (see Figure 6) that ligands can displace the equilibrium between the different G-quadruplex structures by specific binding to a certain loop arrangement.

In general, the rate of the peroxidation reaction was higher for DNAzymes that bound more tightly to hemin (see Tables 5 and 6). In buffers that lack ammonium cation, such as Buffers A, B and C, the rate of product formation approached zero after only two minutes using G**1**, G**6** and G**8** as catalysts. Because greater than 97% of the oxidation substrate, ABTS, remained nonoxidized after two minutes, the dramatic decrease in reaction rate is not due to reduction in substrate concentration. The dissociation constants of the hemin/DNAzyme complexes were inversely proportional to their turnover numbers (TONs; defined

(27) (a) Lee, J. Y.; Okumus, B.; Kim, D. S.; Ha, T. *Proc. Natl. Acad. Sci. U.S.A* **2005**, *102*, 18938–18943. (b) Ying, L. M.; Green, J. J.; Li, H. T.; Klenerman, D.; Balasubramanian, S. *Proc. Natl. Acad. Sci. U.S.A.* **2003**, *100*, 14629–14634. (c) He, Y. J.; Neumann, R. D.; Panyutin, I. G. *Nucleic Acids Res.* **2004**, *32*, 5359–5367. (d) Li, J.; Correia, J. J.; Wang, L.; Trent, J. O.; Chaires, J. B. *Nucleic Acids Res.* **2005**, *33*, 4649–4659.

(28) (a) Seenisamy, J.; Rezler, E. M.; Powell, T. J.; Tye, D.; Gokhale, V.; Joshi, C. S.; Siddiqui-Jain, A.; Hurley, L. H. *J. Am. Chem. Soc.* **2004**, *126*, 8702–8709. (b) Rezler, E. M.; Seenisamy, J.; Bashyam, S.; Kim, M. Y.; White, E.; Wilson, W. D.; Hurley, L. H. *J. Am. Chem. Soc.* **2005**, *127*, 9439–9447.

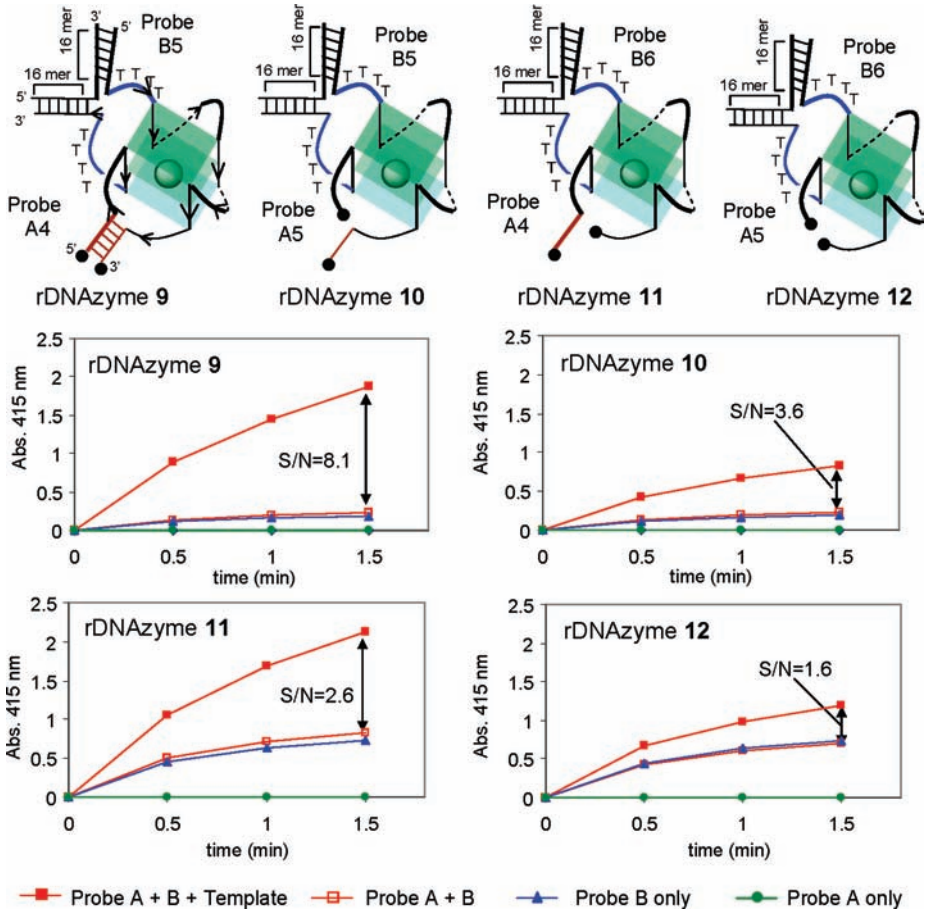

Figure 13. The number of base pairs between probe A or B, and the template is 16 in rDNAzymes **9**−**12**. Split G-quadruplex probes (A and B) which have longer analyte recognition arms are more sensitive in discriminating between the presence and absence of DNA than rDNAzymes which have a shorter recognition arm (compare rDNAzymes **1**, **6**−**8** in Figure 12 with analogous structures rDNAzymes **9**−**12**).

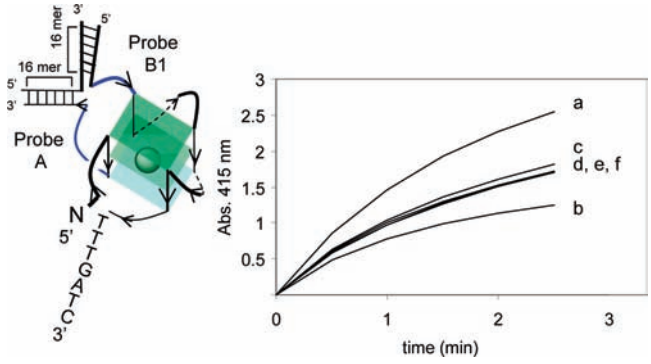

Figure 14. Investigations into the effect of the 5′-end sequence context and length of probe A (split probe that contains only one G-tract) on the speed of the DNAzyme-catalyzed peroxidation reaction. Probe A which contains 5′-end sequence that is complementary to the 3′-end of probe B affords the most proficient peroxidation catalyst (compare entry a with b or d).

in this context as the number of moles of substrate that a mole of catalyst can convert before becoming inactivated). TONs are greater than 1393, 1097 and 565 min^{-1} in Buffer D (excess NH_4^+) for G**1**, G**6** and G**8**, respectively,[29] whereas in Buffers A, B or C, the TONs are less than or equal to 97, 131, and 91 min^{-1} for G**1**, G**6** and G**8** respectively.

(29) To obtain TONs for G**1**, G**6** and G**8**, a cuvette with a pathlength of 1 mm was used so that absorbance values were less than 3.5. See Supporting Information for spectra.

Table 7

probe A	*v* (μM/min)
a: *N* = GATCAAT-5′	47.7
d: *N* = TTTTTTT-5′	34.9
f: *N* = T-5′	33.9
c: *N* = AGCTGAT-5′	33.3
e: *N* = −CAAT-5′	32.6
b: No base	26.9

The higher initial rates of reaction and higher turnover numbers obtained when ammonium cations are present in the buffer can be due to a general acid−base catalysis that is mediated by the ammonium cation or it could be that when ammonium cation is located between the G-quartet planes, the resulting DNAzymes are better enzymes than the case with sodium or potassium (i.e., ammonium ion influences catalysis indirectly by affecting structure and/or dynamics). An alternative hypothesis to explain the low TON observed in buffers that contained either excess potassium or sodium is; the presence of either potassium or sodium cations enhances the degradation of the G-quadruplex DNAzymes or hydrogen peroxide reagent. To shed more light on the role of monovalent cation on TONs, we investigated the peroxidation reactions in a buffer that contained fixed concentration of potassium ion (50 mM) and increasing concentrations of ammonium ions (0−250 mM) (see Figure 8). The addition of increasing amounts of ammonium ions to a buffer containing fixed amounts of potassium ions resulted in an increase in the TONs and initial rate of reaction.

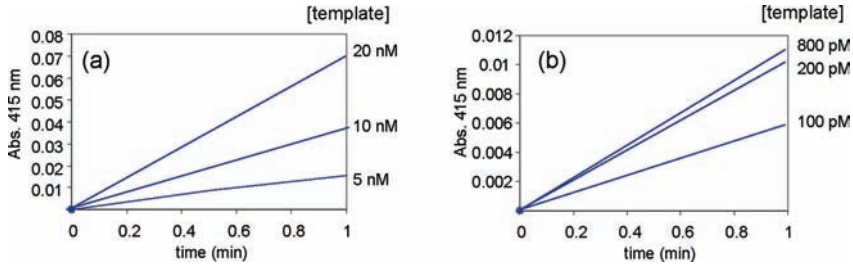

Figure 15. Detection of DNA analytes with TeHyP split G-quadruplex probes. The *y*-axis represents the absorbance of the peroxidation product ($ABTS^{1-}$).Conditions: (a) [probe A] = 50 nM, [probe B] = 25 nM, buffer: Buffer D (excess NH_4^+); (b) [probe A] = 500 pM, [probe B] = 250 pM, buffer: Buffer D (excess NH_4^+); temperature = 20 °C. DNA used = B5, A4 and T2.

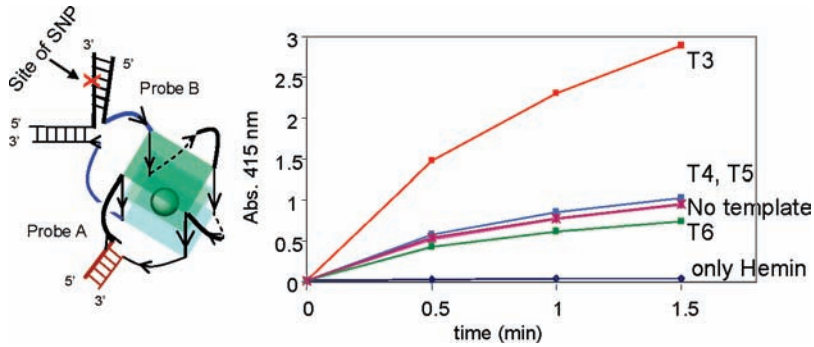

Figure 16. TeHyP split G-quadruplex probes can detect single nucleotide polymorphism. rDNAzymes were reconstituted by mixing probes A, B and various DNA analytes that differed by only a single nucleotide. The time course absorbance of the peroxidation product, $ABTS^{1-}$, indicates that the rDNAzyme that is reconstituted by the perfectly matching template (**T3**) is catalytically more proficient than those formed by templates containing a single nucleotide mismatch site (**T4**, **T5** and **T6**). Probes = A1 and B1.

Interestingly, buffers containing equal amounts of ammonium ions (150 mM) but different amounts of potassium ions (0 and 50 mM) had the same initial rates of reaction but different turnover numbers (the presence of potassium ion decreased TONs). If the decreased TONs in the presence of potassium is due to the inactivation of the hydrogen peroxide reagent, then the addition of extra hydrogen peroxide should restart the oxidation reaction. On the other hand, if the decreased TONs in the presence of potassium is due to the oxidation of the G-quadruplexes, which would lead to the destruction of the quadruplex structure,[30] then the addition of DNAzyme to the stalled reaction will restart the peroxidation reaction. Addition of fresh G-quadruplex DNAzyme (G**8**) to the reaction mixture after it had stalled (see Figure 9) resulted in the resumption of ABTS oxidation. On the contrary, addition of fresh batch of hydrogen peroxide to the stalled oxidation reaction did not reactivate catalysis; providing evidence that the decrease in the peroxidation reaction rate is due to the inactivation of the peroxidase DNAzyme. We conclude that the G-quadruplex structures that contain ammonium ion as the central cation are more resistant to oxidative degradation than those that contain either sodium or potassium.

Effect of the size of loops 1 and 2 on DNAzyme catalysis: When two G-rich probes associate to form a G-quadruplex DNAzyme, two major boundaries are formed (see Figure 1). How does the structure or sequence context at the boundary site affect the enzymatic proficiency of the reconstituted DNAzyme?

In order to answer this question, we studied the effect of loop size and loop sequence content (see Figure 10) on the catalytic proficiencies of the peroxidase-mimicking DNAzymes. The size of loop 1 affects the thermal stability of the G-quadruplexes but not the enzymatic efficiencies (Figure 10). Although G**11** (T_m = 61.4 °C) is more stable than both G**8** (T_m = 59.0 °C) and G**10** (T_m = 57.1 °C), the three DNAzymes (G**11**, G**8** and G**10**) catalyze the oxidation of ABTS at similar rates (Figure 10a). On the other hand, the size of loop 2 affects both the thermal stability and the enzymatic proficiency of the DNAzymes studied. Increasing the size of loop 2 results in a decrease in thermal stability (compare G**8** and G**9** with a T_m of 59.0 and 65.1 °C, respectively) but improves the resulting enzymatic efficiency of the DNAzymes (Figure 10b); The initial velocity of ABTS oxidation by G**8** is 2.7 times higher than that of G**9** (160.8 vs 58.9 μM/min; Table 6).

The sequence context of loop 2 is also an important determinant of the catalytic efficiencies of the DNAzymes studied. DNAzymes that contain thymidines in loop 2 are better enzymes than those that contain adenines or cytosines. In the case of loop 2 that consists of cytosines (G**14**), no enzymatic activity was observed (Figure 10a). This study is the first that has systematically looked at the effect of the sequence context (natural nucleotides) and loop size of loops 1 and 2 on the catalytic proficiency of peroxidase-mimicking DNAzymes.

Detection of DNA Analytes Using Different DNAzyme Architecture. The foregoing investigations were initiated to shed light on the key structural features of a reconstituted DNAzyme (rDNAzyme[31]) that are most important for enzymatic proficiency. Our data indicates that the architecture of loop 2 is critical for the enzymatic efficiency of peroxidase-mimicking DNAzymes (Figure 10). In agreement with this data, the architecture of loop 2 in DNAzymes that were reconstituted from two split probes and a DNA template also impacted the

(30) For examples of 8-oxoguanine substitution in G-quadruplex structures, see: Gros, J.; Rosu, F.; Amrane, S. De Cian, A. Gabelica, V.; Lacroix, L.; Mergny, J. L. *Nucleic Acids Res.* **2007**, *35*, 3064−3075; (b) Benz, A.; Hartig, J. S. *Chem. Commun.* **2008**, 4010–4012.

(31) r denotes reconstituted.

enzymatic efficiency of the reconstituted enzymes (Figure 11); reconstituted G-quadruplex rDNAzyme **1** (loop 2 contains a total of 8 Ts) was a better peroxidase enzyme than rDNAzyme **2** (the quadruplex structure adjoins a duplex region). Interestingly, the asymmetry of loop 2 also impacted the enzymatic proficiency of the rDNAzymes (compare rDNAzyme **4** with rDNAzyme **5**, Figure 11).

The signal-to-noise ratios[32] of the different probe combinations ranged from a best of 3.4 (for rDNAzyme **5**) to unimpressive values of 1.8 and 1.6 (for rDNAzymes **2** and **3**). Despite the fact that probe A and probe B had a region of sequence complementarity (colored brown in Figure 11), the background noise, i.e. the signal in the absence of DNA template did not originate from the nontemplated recombination of probes A and B, *vide infra*. The majority of the background noise arose from signals generated from G-quadruplex structures formed by probe B alone (see Figure 12 and Supporting Information, Figure S22). This is further validated by the observation that the background noises for rDNAzyme **7** and **8** are greater than that of rDNAzyme **1**, although the probes that reconstitute into rDNAzyme **1** have regions of sequence complementarity, whereas those of rDNAzymes **7** and **8** do not have regions of sequence complementarity.

Interestingly, the background noise of rDNAzyme **1** and **6** are similar in value but the signal in the presence of template for rDNAzyme **1** is higher (1.8 times) than for rDNAzyme **6**. This validates our initial assumption that the duplex domain (colored brown in Figure 12), which forms from the complementary sequences between probe A and probe B, helps in the proper folding of the peroxidase G-quadruplex structure. In order to reduce the background noise further, we designed a second set of rDNAzymes with longer sequences that were complementary to the target DNA analyte. Because the entropic cost of folding longer sequences is higher than that for shorter sequences, we reasoned that when the length of probe B is increased, it will have a lower propensity to fold into intermolecular G quadruplexes (which is the source of background noise).[33] In line with our hypothesis, increasing the number of base pairing between the separate probes A and B, and the target DNA analyte resulted in a dramatic reduction in background noise and hence a better signal-to-noise ratios for the rDNAzymes (compare rDNAzyme **1** to **9**, **6** to **10**, **7** to **11** and **8** to **12**; Figures 12 and 13).

Thermal denaturation experiments of probes B**4** and B**5** confirmed that the G-rich probes that contain additional sequences after the 3′-end G-tract (for example probe B**5**) do not form intermolecular G-quadruplexes (evidenced by lack of melting transition when the denaturation experiment is monitored at 260 or 295 nm: see Supporting Information, Figure S23) whereas probes whose 3′-end contains G-tract (for example B**4**) form G-quadruplexes (see Supporting Information, Figure S23). These sets of data explain the origin of the correlation between 3′-end sequence of probe B and background noise.

The absorption data in Figure 13 also reveal a new observation; placing additional DNA sequences after the G-tract at the 5′-end of probe A accelerates the peroxidation reaction (compare rDNAzyme **11** with **12**). To shed more light on this interesting observation, we investigated the effect of various sequence context and lengths at the 5′-end of probe A (see: Figure 14).

These are important observations related to catalysis: (i) Appending a duplex motif next to the G-quadruplex region leads to the best enzymatic system; in Table 7 entry (a), the 5′-end of probe A is complementary to the 3′-end of probe B whereas in entries (b) and (d), the 5′-ends of probe A are not complementary to the 3′-end of probe B. Because the peroxidation reaction is faster in entry (a) than entries (b) and (d), we conclude that the rate enhancement is due to the duplex moiety. (ii) An extra nucleotide after the G-tract at the 3′-end of probe A gives a catalytically more proficient enzyme than when the 3′-end ends with the G-tract. Additional nucleotides after the first extra nucleotide do not provide additional rate enhancements (compare entries (c), (e) and (f)).

Detection of DNA (Limit of Detection and SNP Analysis). The motivation for carrying out the aforementioned experiments was to discover the salient design principles that would facilitate the colorimetric detection of bioanalytes using split DNA probes. With the important information gleaned from our studies, we next investigated the detection of various DNA concentrations using our best probe design (rDNAzyme **9**). Pleasingly, the new optimal probes allowed the colorimetric detection of picomolar concentrations of target DNA in a Buffer D (excess NH_4^+), see Figure 15. These probes could also discriminate between single mismatch polymorphisms; the absorption signal from perfectly matching template was significantly higher than for single mismatches (see Figure 16).

Conclusion

The foregoing experiments have shed light on the important architectural features that are required for separate probes that reconstitute into active DNAzyme catalysts for nucleic acid sensing. We have shown that the loops that connect the G3-tracts in a G-quadruplex structure can be replaced with a stem−loop or loop−stem−loop motif without destabilizing the resulting quadruplex structure.[34] This work complements the study done by Fox which showed that the loops that connect G-tracts in quadruplexes can be replaced with non-nucleosidic linkages and the resulting G-quadruplex structures were more stable than their nucleosidic analogues.[35] A significant result of this study is the demonstration that the addition of hemin to the DNAzymes G**1**, G**5** and G**8** leads to a blue shift in the CD spectra of the G-quadruplex DNAzymes, indicating a probable conformational transition from antiparallel to parallel/mixed-type structures in the aforementioned G-quadruplexes. On the basis of this observation, we conclude that hemin preferentially binds to either the parallel and/or mixed-type G-quadruplexes, and therefore, strategies that lead to the stabilization of parallel G-quadruplex structures might also result in higher affinity of the G-quadruplexes for hemin. Many reports that use G-quadruplex peroxidase-mimicking DNAzymes to detect analytes use buffers that contain excess potassium. This work has however demonstrated that G-quadruplex peroxidases decompose faster in buffers that contain excess potassium or sodium cations than those that contain excess ammonium cation. It, therefore, appears that the majority of peroxidase-mimicking G-quadruplex assays might have been done under less optimum conditions. A significant observation of this paper is the realization that both the sequence content and length of the sequences that flank the G-tract segment of G-quadruplex probes

(32) Defined as ratio of absorbance in the presence of template divided by absorbance in the absence of template after 2.0 min.
(33) The extra sequences do not have to contain G-tracts as this would increase the propensity to fold into intermolecular G-quadruplexes.
(34) Fox has shown that the extension of all of the three loops of G-quadruplexes into duplexes leads to destabilization. See: Risitano, A.; Fox, K. R. *Org. Biomol. Chem.* **2003**, *1*, 1852−1855.
(35) Risitano, A.; Fox, K. R. *Nucleic Acids Res.* **2004**, *32*, 2598–2606.

significantly affect both enzymatic catalysis and background noise. We have also demonstrated that one can use a proximal duplex motif to facilitate the folding of G-quadruplex DNAzyme and hence affect the enzymatic efficiency of the reassembled G-quadruplex DNAzyme. The discovery of these salient architectural designs has facilitated the colorimetric detection of picomolar concentrations of target DNA analytes using label-free DNA probes. It is anticipated that the strategies described in this paper will find usage in other nanotechnology applications that use G-quadruplexes as enzymes or structural scaffolds.[36] We hope that this study opens up a debate into how peroxidase-mimicking G-quadruplexes can be stabilized against oxidative damage.

Acknowledgment. This work was supported by the University of Maryland, College Park.

Supporting Information Available: Additional melting curves, titration curves and determination of equations for calculation of peroxidation velocities, and complete ref 5b. This material is available free of charge via the Internet at http://pubs.acs.org.

(36) Davis, J. T. *Angew. Chem., Int. Ed.* **2004**, *43*, 668–698.

JA902951B